The Sensitivity of Simulated River Discharge to Land Surface Representation and Meteorological Forcings

STEFANO MATERIA

Centro Euro-Mediterraneo per i Cambiamenti Climatici, Bologna, Italy

PAUL A. DIRMEYER AND ZHICHANG GUO

Center for Ocean–Land–Atmosphere Studies, Calverton, Maryland

ANDREA ALESSANDRI

Centro Euro-Mediterraneo per i Cambiamenti Climatici, Bologna, Italy

ANTONIO NAVARRA

Centro Euro-Mediterraneo per i Cambiamenti Climatici, and Istituto Nazionale di Geofisica e Vulcanologia, Bologna, Italy

(Manuscript received 10 February 2009, in final form 21 September 2009)

ABSTRACT

The discharge of freshwater into oceans represents a fundamental process in the global climate system, and this flux is taken into account in simulations with general circulation models (GCMs). Moreover, the availability of realistic river routing schemes is a powerful instrument to assess the validity of land surface components, which have been recognized to be crucial for the global climate simulation. In this study, surface and subsurface runoff generated by the 13 land surface schemes (LSSs) participating in the Second Global Soil Wetness Project (GSWP-2) are used as input fields for the Hydrology Discharge (HD) routing model to simulate discharge for 30 of the world's largest rivers. The simplest land surface models do not provide a good representation of runoff, and routed river flows using these inputs are affected by many biases. On the other hand, HD shows the best simulations when forced by two of the more sophisticated schemes. The multimodel ensemble GSWP-2 generates the best phasing of the annual cycle as well as a good representation of absolute values, although the ensemble mean tends to smooth the peaks. Finally, the intermodel comparison shows the limits and deficiencies of a velocity-constant routing model such as HD, particularly in the phase of mean annual discharge.

The second part of the study assesses the sensitivity of river discharge to the variation of external meteorological forcing. The Center for Ocean–Land–Atmosphere Studies version of the SSiB model is constrained with different meteorological fields and the resulting runoff is used as input for HD. River flow is most sensitive to precipitation variability, but changes in radiative forcing affect discharge as well, presumably because of the interaction with evaporation. Also, this analysis provides an estimate of the sensitivity of river discharge to precipitation variations. A few areas (e.g., central and eastern Asia, the Mediterranean, and much of the United States) show a magnified response of river discharge to a given percentage change in precipitation. Hence, an amplified effect of droughts as indicated by the consensus of climate change predictions may occur in places such as the Mediterranean. Conversely, increasing summer precipitation foreseen in places like southern and eastern Asia may amplify floods in these poor and heavily populated regions. Globally, a 1% fluctuation in precipitation forcing results in an average 2.3% change in discharge. These results can be used for the definition and assessment of new strategies for land use and water management in the near future.

Corresponding author address: Stefano Materia, Centro Euro-Mediterraneo per i Cambiamenti Climatici, Viale Aldo Moro, 44–40127 Bologna, Italy.
E-mail: stefano.materia@cmcc.it

DOI: 10.1175/2009JHM1162.1

1. Introduction

In recent years, the important role played by the land surface in the global climate system has been recognized (Koster et al. 2006), and increasingly sophisticated land surface schemes (LSSs) have been developed for general circulation models (GCMs; e.g., Bonan et al. 2002; Alessandri et al. 2007). Not only is an accurate simulation of the land surface state crucial for the skill of seasonal and weather forecasts (Ferranti and Viterbo 2006; Fischer et al. 2007; Alessandri and Navarra 2008), but also it can improve the understanding and the prediction of flood damage potential (Takeuchi 2001). Soil wetness is a boundary condition for the atmosphere; it affects land surface temperature and flux and plays an essential role in the partitioning of convective fluxes between sensible and latent heat. Soil moisture's status is a fundamental initial condition for climate predictability on seasonal to annual time scales (AMS Council 2001). Nevertheless, it is well observed only over very limited areas (e.g., Robock et al. 2000). This deficiency exists primarily because in situ measurement of soil moisture (as well as snow mass and soil heat content) is difficult to accomplish, and remote sensing techniques are not always effective (Dirmeyer et al. 2006).

However, many observational datasets are available for river discharge, which represent the final stage of the land surface water cycle before draining into the oceans. Consequently, river routing schemes (RRSs) can be validated more readily than land surface schemes. Moreover, since river routing schemes are forced by runoff generated by LSSs, they can be used to integrate the simulated runoff into river discharge at gauging stations over selected river basins. Thus, it is possible to evaluate the water budget simulated over the corresponding drainage area by comparing simulated discharges with observation (Decharme and Douville 2007).

In this study, outputs from 13 land surface schemes participating in the Second Global Soil Wetness Project (GSWP-2; Dirmeyer et al. 2006; see Table 1) are used as forcings for the Hydrology Discharge (HD) model (Hagemann and Dümenil 1998a). The response of river discharges produced by HD to the different surface and subsurface runoff values is evaluated. Moreover, the quality of meteorological forcing data has a strong influence on the simulation of land surface components of the hydrological cycle (Guo et al. 2006). GSWP-2 included a number of sensitivity experiments in which LSSs are forced by different precipitation and radiation fields. Thus, the response of discharge to changes in forcing data and surface parameters is assessed for the HD model, using the GSWP-2 sensitivity experiments applied to the SSiB LSS (Xue et al. 1991), updated by Dirmeyer and Zeng (1999). The simulated discharges consequently provide an indirect quality check for the LSSs themselves.

2. The GSWP-2 dataset

GSWP-2 is an ensemble modeling activity whose goal is to provide estimates of soil moisture, water and energy balance components, and surface and subsurface variables by integrating uncoupled land surface schemes using meteorological forcings based on a combination of reanalysis and observations. GSWP-2 produced land surface water and energy cycle component estimates over the period 1986–95.

The model simulations for GSWP-2 were conducted globally over land on a $1° \times 1°$ regular grid, using the same land sea mask, over the 10-yr period mentioned above. Data were reported at a daily interval. A GSWP-2 multimodel analysis (MMA) was produced by arithmetically averaging the output fields generated by the 13 LSSs shown in Table 1 (Dirmeyer et al. 2006). It includes uncertainty estimates for all the fields based on intermodel spread. The integrated LSSs were not coupled to atmospheric models but were forced with the best possible observationally based estimates of near-surface meteorology, radiation, and precipitation.

To aggregate the uninterrupted space–time availability of the reanalysis and the accuracy of gridded observational data, a combination of the two was used to force the LSSs. Moreover, where station observations were scarce, satellite-estimated precipitation from the Global Precipitation Climatology Project (GPCP; Huffman et al. 1997) was applied. This hybridization process has been developed, tested, and documented by Dirmeyer and Tan (2001). For GSWP-2 the baseline forcing data used were the National Centers for Environmental Prediction–Department of Energy (NCEP–DOE; Kanamitsu et al. 2002) reanalysis data (Zhao and Dirmeyer 2003). Vegetation and soil variables were specified by the International Satellite Land-Surface Climatology Project (ISLSCP) Initiative II dataset (II2; Hall et al. 2006), and each participating LSS used the parameterization appropriate to its formulation.

Eleven models contributed fully to the MMA (Table 1), each generating a complete set of land surface state variables for the 10-yr period 1986–95. Sland and BucketIIS were excluded because they do not calculate many of the mandatory variables (however, they were run as reference models), while LaD and ORCHIDEE did not contribute to the MMA estimate of normalized soil wetness but provided other outputs.

These models portray a wide spectrum of the complexity in representation of surface processes. BucketIIS

TABLE 1. LSSs participating in GSWP-2. Vertical structure shows soil layers for water (W) and temperature (T), and the maximum number of snow layers (S). VISA and CLM2-TOP have different time steps for energy (E) and soil hydrology (S). Sland and BucketIIS are not included in the multimodel analysis. From Dirmeyer et al. (2006).

Name	Institute	Nation	Time step	Vertical structure	Recent references
CLM2-TOP	University of Texas	USA	1hE 5mS	10W 10T 5S	Bonan et al. (2002); Niu and Yang (2003)
HY-SSIB	Goddard Space Flight Center (GSFC)	USA	30 min	3W 2T 2S	Mocko and Sud (2001)
ISBA	Météo-France Centre National de Recherches Météorologiques (CNRM)	France	5 min	3W 2T 1S	Etchevers et al. (2001)
Mosaic	NASA GSFC/ Hydrological Sciences Branch (HSB)	USA	30 min	3W 2T 1S	Koster and Suarez (1992)
MOSES2	Met Office	UK	30 min	4W 4T 1S	Essery et al. (2003)
Noah	National Oceanic and Atmospheric Administration (NOAA)–NCEP–Environmental Modeling Center (EMC)	USA	15 min	4W 4T 1S	Ek et al. (2003)
NSIPP	NASA GSFC–Global Modeling and Assimilation Office (GMAO)	USA	20 min	3W 6T 3S	Koster et al. (2000); Ducharne et al. (2000)
SiBUC	Kyoto University	Japan	1 h	3W 2T 1S	Online
COLASSiB	IGES (COLA)	USA	30 min	6W 6T 1S	Dirmeyer and Zeng (1999)
SWAP	Russian Academy of Sciences–IWP	Russia	3 h	2W 1T 1S	Gusev and Nasonova (2003)
VISA	University of Texas	USA	3hE 5mS	10W 10T 5S	Yang and Niu (2003); Niu and Yang (2003)
LaD	NOAA/GFDL (Geophysical Fluid Dynamics Laboratory)	USA	30 min	1W 18T 1S	Milly and Shmakin (2002a,b)
ORCHIDEE	Institute Pierre Simon Laplace (IPSL)	France	1 h	4W 7T 1S	Krinner et al. (2005)
Sland	University of Maryland	USA	20 min	1W 2T 0S	Zeng et al. (2005)
BucketIIS	University of Tokyo	Japan	3 h	1W 1T 1S	Manabe (1969)

and LaD stem from the first-generation bucket models, with a very simple depiction of vegetation and unsatisfactory treatment of surface energy balance. On the other hand, CLM2-TOP, MOSES2, and ORCHIDEE are examples of third-generation LSSs, which include a sophisticated representation of vegetation functioning, carbon cycle, and biogeochemistry. The remaining models belong to the second-generation schemes, which adequately treat the surface energy balance and the physical effect of vegetation on the water cycle through the introduction of stomatal resistance parameterization (Guo and Dirmeyer 2006).

The complete set of outputs at a regular 1° resolution includes energy balance components (shortwave and longwave radiation, heat fluxes, energy of fusion and sublimation), water balance components (rainfall and snowfall rate, total evapotranspiration, runoff, etc.), surface and subsurface state variables (temperature of soil and snow surface, albedo, snow surface equivalent on ground and canopy, soil temperature, moisture and wetness, etc.), and all the terms constituting the evaporation process. The MMA is a complete dataset, not subject to systematic errors often affecting individual models.

3. The HD river routing scheme

In this study, we use the Hydrology Discharge river routing scheme (Hagemann and Dümenil 1998a), which was implemented in ECHAM5 (Roeckner et al. 2003). The model works in offline mode, uncoupled from the atmospheric component.

This scheme separates the gridpoint lateral water flow into three processes: overland flow, base flow, and river flow. The first one takes its input from the runoff and the second one is fed by drainage (water flowing in deep soil layers), while flow coming from other grid boxes contributes to river flow. The sum of these processes equals the outflow from a grid point. Input fields are generated by the land surface scheme implemented in GCMs and are transferred to HD once per day to provide daily outputs.

The HD model uses the linear reservoir approach, where the outflow Q from a reservoir is proportional to its content S. The proportionality between the two values is given by the retention coefficient k, defined as the average residence time of the water into a reservoir (Singh 1988):

$$Q(t) = \frac{S(t)}{k}. \tag{1}$$

A general reservoir has to satisfy the continuity equation that relates Q to the inflow into the reservoir:

$$\frac{dS(t)}{dt} = I(t) - Q(t). \tag{2}$$

These two equations lead to a linear differential equation for the discharge Q, with one parameter k:

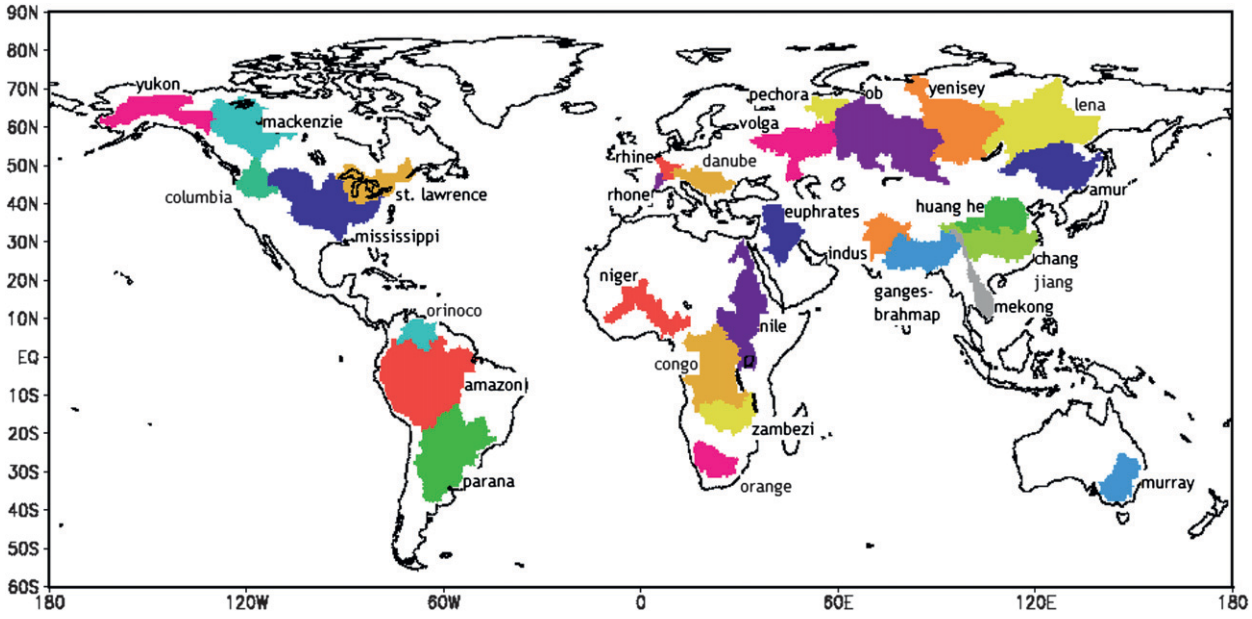

FIG. 1. Watersheds of the 30 large rivers named in Table 2.

$$k\frac{dQ(t)}{dt} = I(t) - Q(t). \tag{3}$$

Base flow is represented by a single linear reservoir, and its retention coefficient k_b is simply a function of the grid box length (Δx, the distance between two adjacent grid points). In contrast, overland and river flow are both characterized by a cascade of n equal reservoirs, and their retention times (k_o and k_r respectively) depend on grid box length and on the topographic gradient between two adjacent grid points.

HD computes the discharge at 0.5° resolution, and a topography dataset was built at this resolution by area-weighted averaging a 5-min global topography dataset from the National Geographic Data Center (Edwards 1989). Consequently, a flow direction parameter was created to produce river catchments. Nevertheless, this procedure is not sufficient for an accurate global discharge simulation because it contains several unrealistic local minima over land. Two smoothing algorithms were necessary to remove these minima, but simulated catchments still differ from real ones; hence, some manual corrections have been performed (Hagemann and Dümenil 1998b).

Figure 1 shows the location of 30 of the largest river basins on earth examined in this study (see also Table 2).

The final parameterization of HD was determined empirically using data from the Torneälven–Kalixälven catchment system, an unmanaged Swedish drainage basin. The empirical factors link the retention times to topography gradient:

$$k_o = \alpha\frac{\Delta x}{\varphi^{0.1}}, \quad n_o = 1, \tag{4}$$

$$k_r = \beta\frac{\Delta x}{(\Delta h/\Delta x)^{0.1}}, \quad n_r = 5, \tag{5}$$

where k_o (order of magnitude 10^0–10^1 days) is the retention coefficient for overland flow; k_r (order of magnitude 10^{-1}–10^0 days) is the same for river flow, both expressed in days; $\Delta h/\Delta x$ is the topographic gradient to the next grid box in flow direction, which replaces the average slope φ within a grid box in the river flow relation; n_i is the number of linear reservoirs for the two type of flows; and α and β are globally constant coefficients, calculated for the Torneälven–Kalixälven catchment basin and extracted for the other world's catchments. Therefore, the corresponding flow velocities v_i (with $i \in \{o, r\}$) of overland and river flow are

$$v_i = \frac{\Delta x}{n_i k_i}. \tag{6}$$

The number of chosen reservoirs n_i is five for river flow and one for overland flow.

Finally, the retention time k_g for base flow is defined as

$$k_g = \frac{t_g \Delta x}{d_0}, \tag{7}$$

where t_g has been set to 300 days globally, while d_0 represents the 0.5° grid box side.

TABLE 2. Gauge station, simulated and actual catchment areas at the river mouth, and location and period of observation to create climatology of discharge for 30 of the largest world rivers.

Basin	Station	Simulated drainage area (10^6 km^2)	Measured drainage area (10^6 km^2)	Lat (°N)	Lon (°E)	Period
Amazon	Obidos	5.835	6.144	−2.25	−55.75	1986–95
Congo	Brazzaville	3.823	3.730	−4.25	15.25	1986–95
Paraná[a]	Timbues	3.805	2.582	−32.75	−60.75	1986–94
Nile	Dongola	3.267	3.255	19.25	30.25	1955–84
Ob	Salekhard	3.119	2.972	66.25	66.25	1986–95
Mississippi	Vicksburg	3.041	3.202	32.25	−91.25	1986–95
Lena	Kusur	2.938	2.306	71.25	127.25	1986–95
Niger	Niamey	2.317	2.262	13.25	2.25	1986–95
Amur	Komsomolsk	2.035	1.930	50.75	137.75	1961–90
Yenisey	Igarka	2.013	2.554	67.75	86.25	1986–95
Zambezi[a]	Katima Mulilo	1.890	1.332	−17.25	24.25	1986–95
Ganges[b]	Harding Bridge	1.878	1.657	24.25	88.75	1985–92
Brahmaputra[b]	Bahadurabad			24.75	89.75	1985–92
Chang Jiang	Hankou	1.750	1.722	30.75	114.25	1957–86
Mackenzie	Arctic Red River	1.734	1.743	67.75	−133.75	1986–95
Euphrates[c]	Hindiya	1.393	0.766	32.75	44.25	1923–72
Volga	Volgograd P.S.	1.366	1.411	48.75	44.75	1986–95
Huang He[a]	Tanglai Qu	1.344	0.945	39.25	106.75	1986–95
St. Lawrence	Cornwall	1.298	1.050	45.25	−74.75	1986–95
Indus[c]	Kotri	1.149	1.081	25.25	68.25	1936–79
Murray	Overland Corner	1.016	1.050	−34.25	140.75	1986–95
Yukon	Stevens Village	0.982	0.848	65.75	−149.75	1986–95
Orange	Vioolsdrif	0.927	0.941	−28.75	17.75	1986–95
Mekong	Mukhadan	0.830	0.805	16.25	105.25	1986–93
Orinoco	Puente Angostura	0.793	0.953	8.25	−63.25	1960–89
Danube	Zimnicea	0.782	0.795	43.75	25.25	1986–95
Columbia	The Dalles	0.674	0.657	45.75	−121.25	1986–95
Pechora	Oksino	0.281	0.322	67.25	52.25	1986–95
Rhine	Lobith	0.180	0.199	51.75	6.25	1986–95
Rhone	Beaucaire	0.082	0.101	43.75	4.75	1986–95

[a] Catchment area is overestimated because the model includes watersheds that are separate in real life.
[b] Catchment area refers to the two rivers together.
[c] Longer climatology due to missing data during 1986–95.

For use with GSWP-2 data, overland flow is supplied by the ''surface runoff'' variable, and base flow by ''subsurface runoff.'' No other variables are used to drive HD. The input fields generated by GSWP-2 in 1° resolution are read and a bilinear interpolation is applied to match them with the 0.5° grid of HD.

4. Experimental design

a. Intermodel comparison

The first stage of the study is an analysis of river discharge forced by surface runoff and drainage (subsurface runoff) generated by the 13 land surface schemes participating in GSWP-2 baseline test B0 (Table 2). As Sland and BucketIIS did not participate in the MMA, they were not taken into consideration for this analysis. All models had been previously run in offline mode for the period 1986–95, driven by meteorological forcings obtained by the hybridization mentioned above. Then, resultant surface and subsurface runoff (Fig. 2) were provided as input to the routing scheme HD to produce river discharge at a global scale. Since GSWP-2 provides variables on a regular 1° × 1° grid, and HD represents river flow at 0.5° resolution, a bilinear interpolation was performed for runoff and drainage.

The ability of each LSS to generate realistic runoff volumes and partition between surface and subsurface runoff can be determined by comparing simulated river discharge and observations. The latter are supplied by the Global Runoff Data Center (GRDC; http://grdc.bafg.de) for the cited 10-yr period. This comparison is presented for selected basins in the following section. Since a few large rivers do not have data for the whole time series, we used a 30-yr or longer climatology to validate discharge for drainage basins with a data coverage shorter than eight years between 1986 and 1995 (Table 2). Simulated discharge was taken at the grid box closest to the actual gauge station.

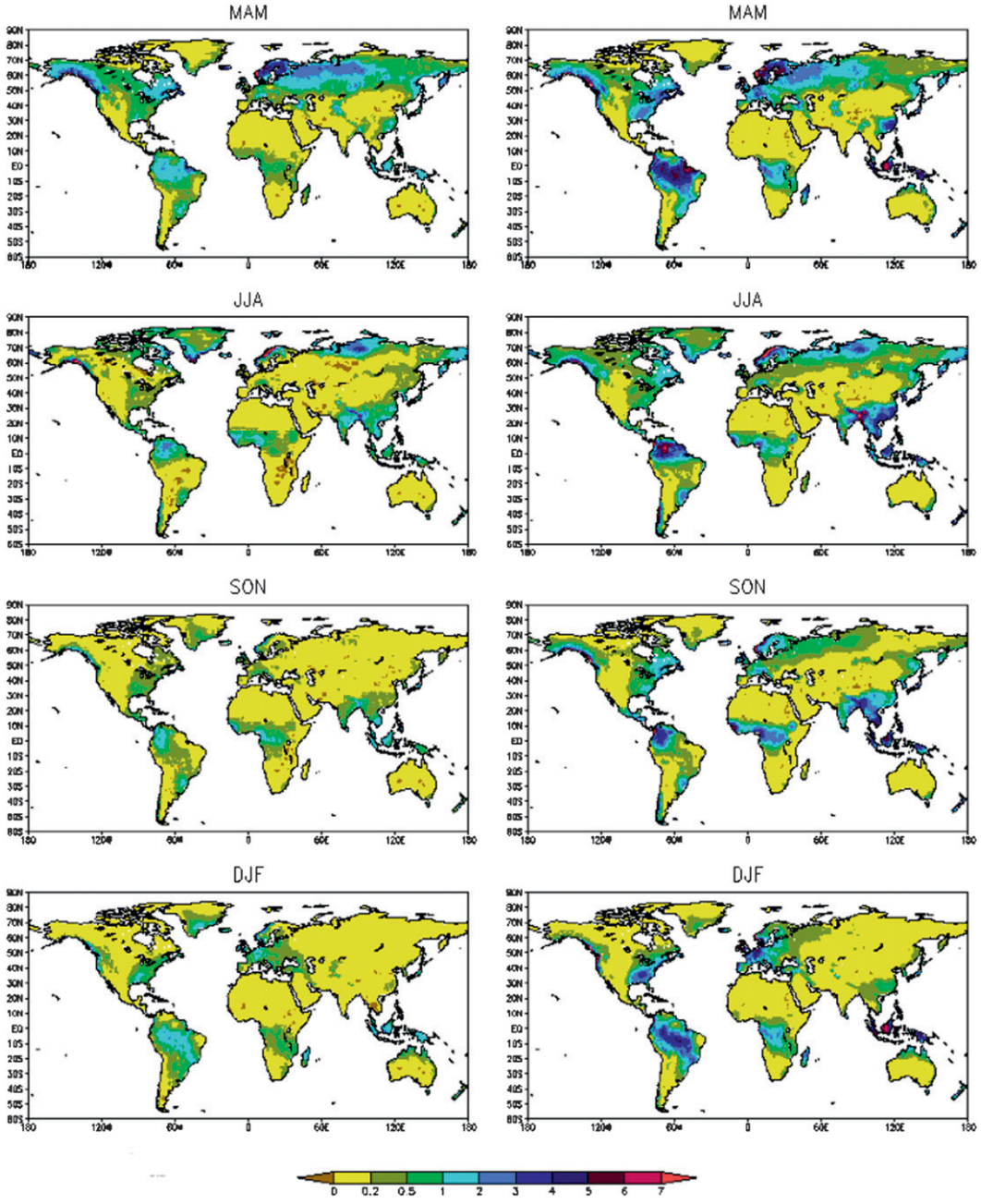

FIG. 2. (left) Surface and (right) subsurface runoff generated by the GSWP-2 multimodel analysis. Seasonal means (mm day^{-1}) for the period 1986–95 are shown.

b. Sensitivity experiments

GSWP-2 provides many diverse meteorological forcing variables and land surface parameters that allow the investigation of the role of external forcing on the simulation of land surface components.

For each set of forcing fields, the GSWP-2 dataset includes runoff estimates that were used as input to HD. The entire set of experiments is described in Table 3. Every experiment tests the sensitivity of discharge to different runoff obtained by varying single or multiple inputs to one LSS. The full set of precipitation and radiation tests was carried out using the SSiB LSS. SSiB provides a nominal representation of the surface–subsurface interface: Guo and Dirmeyer (2006) showed that the RMSE between modeled soil moisture and observations is in the middle among other typical models participating in GSWP-2. Since runoff is intimately related to soil

TABLE 3. Description of GSWP-2 sensitivity experiment and comparison with baseline experiment. From Guo et al. (2006).

Name	Description	Comparable data used in B0
B0	Baseline integration (meteorological forcing and vegetation dataset used in the sensitivity test are the same as the B0 experiment except the variables indicated below)	See Guo and Dirmeyer (2006, their Table 2) for meteorological forcing used in B0
M1	All NCEP–DOE meteorological data without hybridization with observational data	All NCEP–DOE meteorological data hybridized with observational data
M2	All ECMWF meteorological data without hybridization with observational data	Same as above
P1	Precipitation from ERA-40 without hybridization	Precipitation from NCEP–DOE hybridized with GPCC and GPCP corrected for wind caused undercatch
PE	ERA-40 precipitation hybridized with GPCC gridded gauge analysis	Same as above
P2	NCEP–DOE precipitation hybridized with GPCC gauge and corrected for wind caused gauge undercatch	Same as above
P3	NCEP–DOE precipitation hybridized with GPCC gauge without adjustment for wind caused gauge undercatch	Same as above
P4	Precipitation from NCEP–DOE without hybridization	Same as above
R1	Radiation from NCEP–DOE reanalysis	Radiation products from SRB
R2	Radiation from ERA-40 reanalysis	Same as above
R3	Radiation from ISCCP	Same as above

moisture, it is reasonable to think that runoff as well is realistically treated by SSiB.

Data from the NCEP–DOE reanalysis (Kanamitsu et al. 2002) drive the B0, P2, P3, and P4 experiments, while precipitation from the 40-yr European Centre for Medium-Range Forecasts (ECMWF) Re-Analysis (ERA-40; Simmons and Gibson 2000) is used in simulations P1 and PE. P1 and P4 are pure reanalysis products, with no observational data integration, whereas PE is hybridized in the same manner as the baseline experiment described in section 2. The two experiments differ in that in this case PE is built using ERA-40 rather than NCEP data, combined with observations from the Global Precipitation Climatology Center (GPCC; Rudolf et al. 1994) and satellite-estimated precipitation from the GPCP. A simpler hybridization constituted by observation and NCEP reanalysis only, without remote sensing adjustment, is used in the P2 and P3 experiments. The latter is not corrected for wind-caused gauge undercatch, which is shown to be a cause of large overestimation, especially at high latitudes (Oki et al. 1999).

Radiation is another driver for land surface variables because it affects the energy budget. Experiments R1 and R2 use surface radiation fields reanalysis from NCEP and ECMWF, respectively, while the International Satellite Cloud Climatology Project (ISCCP; Rossow and Zhang 1995) supplies radiation data for the R3 simulations. They are all compared to satellite-based radiation from Surface Radiation Budget (SRB) dataset (Stackhouse et al. 2000).

Moreover, SSiB has been subjected to the M1 and M2 experiments, where the set of meteorological data is taken entirely from NCEP reanalysis and ERA-40, respectively. In these cases, air temperature and humidity, surface radiation, wind speed, and precipitation are only reanalysis products, with no observational adjustment.

5. Results

a. Intermodel comparison

Figures 3 and 4 show the mean annual cycle of discharge for 12 of the largest rivers in the world, obtained from runoff generated by 13 land surface schemes contributing to GSWP-2 and to the MMA itself. Discharge is calculated at the grid point corresponding to the actual gauge station (Table 2).

There are differences in skill among regions as well as among models: a few drainage basins are shown to be more difficult to represent. The Paraná (Fig. 3c) shows a flat pattern in the observations, while simulations driven by the majority of the models exhibit a peak during April and May, slightly late with respect to the end of rainy season. This would be expected in an area where the contribution of subsurface runoff is predominant according to most LSSs (Fig. 2). However, although HD accounts for the presence of wetlands (Hagemann and Dümenil 1998b), its retention times seem to be too short to well represent swampy areas. In fact, the upper Paraná (Paraguay river) flows into a region called Pantanál, the world's largest contiguous area of wetlands, a flat landscape that acts as a buffer delaying and spreading the discharge over the year (Barros et al. 2004). For the Saint Lawrence (Fig. 3f), most schemes drive a simulated discharge maximum in April or May because of the large amount of snow melting in the northeast United States, Ontario, and Quebec. Actually, since the Saint Lawrence's catchment includes the Great Lakes, water is stored and

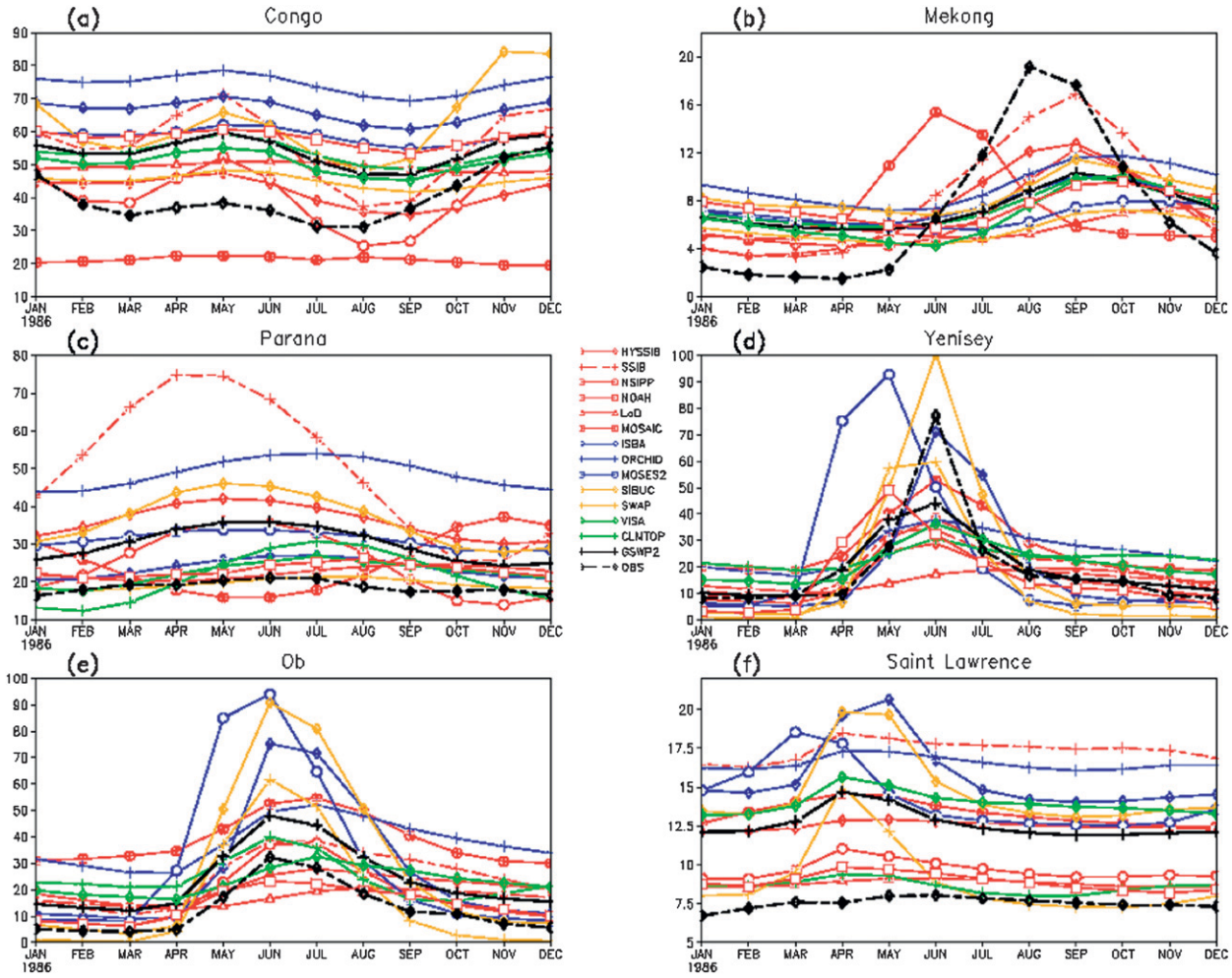

FIG. 3. Climatological monthly mean discharges for six of the analyzed rivers. The HD model is forced by 13 land surface schemes participating in GSWP-2. All values are expressed in thousands of cubic meters per second.

slowly released to the river (Vörösmarty and Sahagian 2000; Branstetter and Erickson 2003), which has a flat annual cycle with a slight peak during the summer. The near totality of the LSSs delays summer discharge peak for rivers flowing in the Indian monsoon area (Ganges, Fig. 4e; Mekong, Fig. 3b). This bias is most likely due to HD, whose time-independent flow velocity is not able to transfer at the right time the runoff released by summer precipitation to the river system. Using another routing scheme, Hanasaki et al. (2008) better replicate the observed values in this region. On the other hand, a few catchments such as the Amazon (Fig. 4a) and Danube (not shown) anticipate the peak with both the routing models.

Other annual cycles are better depicted by HD, as shown by the multimodel-driven simulation, especially at high latitudes. The phase is usually well represented by the experiments forced by the GSWP-2 MMA. However, the routing scheme performs very differently when constrained by individual LSSs. ISBA, for instance, drives a very good simulation at high latitudes (Figs. 3d, 3e, and 4c), while SSiB looks better for tropical rivers (Figs. 3b and 4a). Noah seems to overanticipate the snow-melting season at high latitudes but performs well elsewhere. On the other hand, HD produces a weak seasonality when forced by a simple surface scheme like LaD and simulates an incorrect annual cycle (e.g., in tropical regions) when driven by Mosaic.

Table 4 shows the root-mean-square deviation between observation and models. The first column describes the MMA absolute error, while the other columns are a percentage deviation from GSWP-2 MMA. Again, the MMA forcing leads to values closer to gauge-station data, but the best performances come from second-generation schemes, like Noah, which shows a particularly fine skill at midlatitudes, and NSIPP, which shows laudable performance everywhere. Third-generation

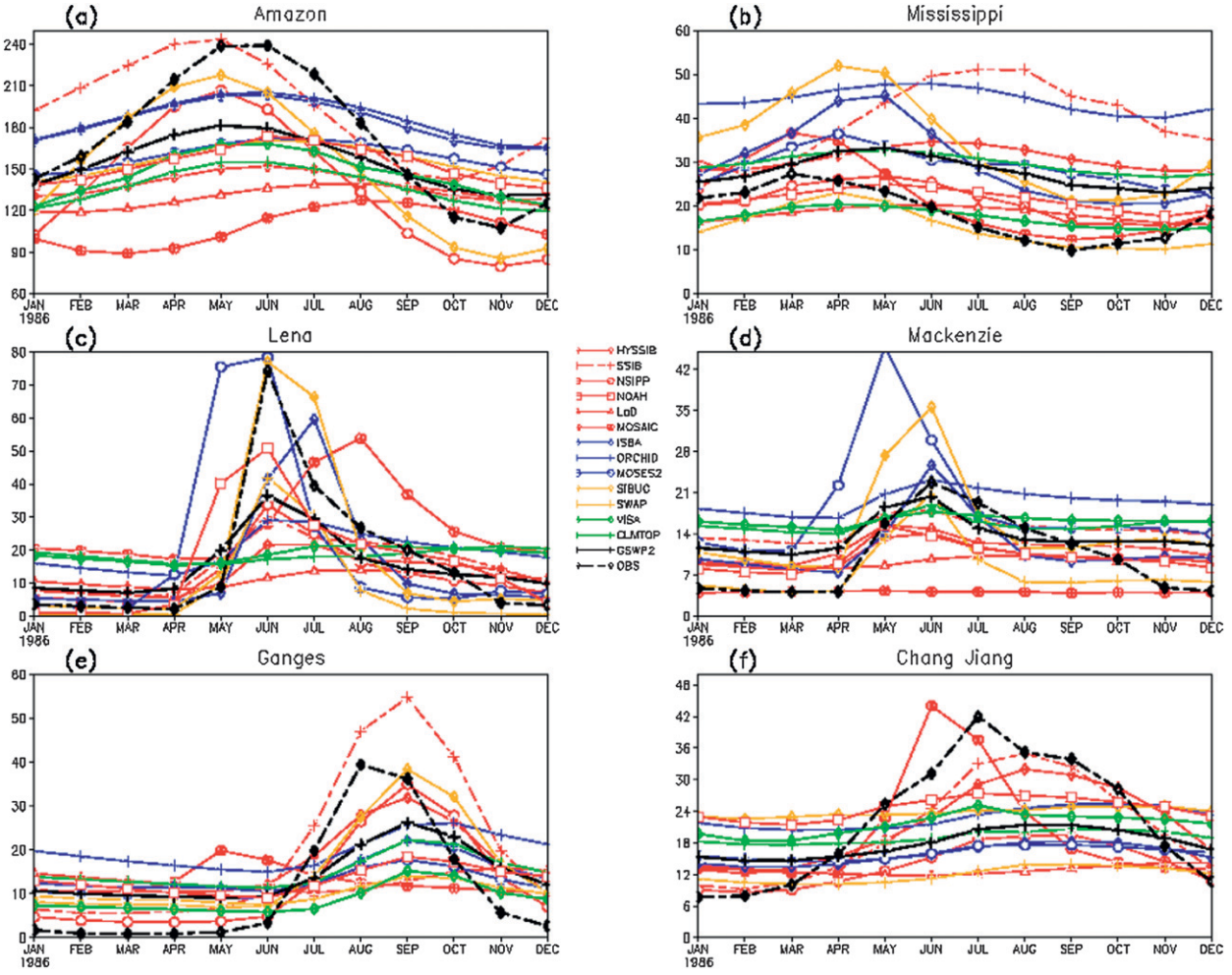

FIG. 4. As in Fig. 3, but with different rivers.

models such as MOSES2 and ORCHIDEE have a poor skill regarding discharge amplitude. Simpler LSSs, other than showing a weak seasonality, are marked by a large root-mean-square error, except for rivers characterized by small intra-annual variability as discussed above. For instance, the inability of LaD to simulate realistically the phasing of runoff leads to a misleadingly good representation when measured by RMSE.

A few rivers such as the Mississippi, the Saint Lawrence, and the Nile are heavily managed for human purposes, with dams regulating discharges. Since in this study rivers are represented as totally natural, their discharges are overestimated in most of the simulations (Figs. 3f and 4b), and their absolute RMSE is large by comparison with measured values (Table 4). Hanasaki et al. (2006) propose a reservoir operation parameterization to take this feature into account and correct seasonal peaks.

Additionally, precipitation is overestimated in GSWP-2 B0, mainly because of overcorrection of precipitation data for wind-caused undercatch of snow (and to a lesser extent rain) at middle and high latitudes (Hanasaki et al. 2008). This is another possible reason why American rivers have high simulated discharge, and a plausible explanation for the streamflow overestimation produced by the almost totality of models at Salekhard (Ob) and Arctic Red River (Mackenzie).

b. *Sensitivity experiments*

After analyzing the control experiment, we used the sensitivity study data from SSiB driven by different radiation, precipitation, and meteorological forcings to generate runoff and force HD. Figure 5 shows a normalized difference between discharge obtained by the sensitivity tests and the control run B0. It is evident that the variation in precipitation fields leads to drastic changes in river discharge, while different radiation fields have a less dramatic impact. Globally, changing precipitation results in a 63% variation of discharge, whereas different

TABLE 4. (first column) Discharge RMSE between observation and GSWP-2. (remaining columns) Land surface scheme percent deviation from the GSWP-2 multimodel analysis.

	GSWP2 ($m^3 s^{-1}$)	NSIPP	Noah	VISA	SWAP	HySSiB	LaD	ISBA	CLM2-TOP	SSiB	SiBUC	MOSES2	Mosaic	ORCHIDEE
Amazon	32 909	114	116	117	124	153	186	102	149	100	79	125	245	106
Congo	15 267	44	119	83	59	52	81	179	102	120	152	132	136	230
Parana	11 788	78	43	37	13	150	39	44	53	302	158	107	93	256
Ob	11 646	47	50	106	112	91	83	180	109	111	228	254	227	220
Mississippi	10 236	43	57	44	42	135	54	122	119	243	165	112	46	256
Lena	12 858	103	97	154	101	131	161	92	164	112	73	164	160	128
Niger	4411	127	78	52	46	79	77	79	68	229	145	112	159	164
Amur	5974	84	101	110	161	74	128	122	166	94	155	217	258	155
Yenisey	10 600	108	149	129	120	135	171	86	157	124	116	267	124	149
Zambezi	1271	46	60	44	48	106	171	141	167	182	140	95	147	281
Ganges	9555	63	125	123	128	93	150	120	127	113	85	116	149	156
Brahmaputra	10 354	101	109	89	76	123	73	94	92	125	118	88	131	123
Chang Jiang	10 341	111	111	127	143	58	145	115	108	41	108	118	84	103
Mackenzie	4868	88	70	149	83	93	112	71	145	123	125	217	161	193
Euphrates	1677	62	87	37	83	143	81	157	105	153	137	123	339	178
Volga	9032	80	44	70	181	85	69	184	108	98	224	232	36	156
Huang He	261	208	50	196	207	310	257	125	413	175	505	157	2700	296
St. Lawrence	5132	42	30	124	51	97	25	162	24	192	146	138	113	175
Indus	2884	—	110	128	123	162	113	140	110	121	134	106	564	168
Murray	1049	39	57	21	19	172	18	67	115	267	64	65	205	375
Yukon	6476	—	107	84	150	108	88	121	113	89	165	186	48	124
Orange	720	24	23	32	28	237	23	103	95	338	101	46	640	384
Mekong	4868	83	117	109	121	62	132	104	105	48	112	125	132	117
Orinoco	16 828	81	111	103	121	101	135	103	111	70	63	117	146	107
Danube	3931	79	62	55	56	134	65	147	129	110	152	127	85	155
Columbia	838	246	117	121	243	163	161	338	138	179	459	439	435	291
Pechora	2325	89	144	155	110	173	195	102	177	135	109	215	204	178
Rhine	2681	103	81	81	66	120	87	115	106	92	121	107	38	118
Rhone	579	84	73	62	61	157	88	116	118	97	131	122	208	146
Average	7288	87	95	100	102	113	117	117	119	126	127	150	160	160

radiation fields vary river outflows only by 6.5% (Table 5). Also, as a further demonstration of the prevalent role of precipitation in driving hydrological processes, tests P1 and M2 show almost identical differences with respect to B0, and P4 and M1 also have extremely similar deviation from baseline experiment. P1 differs from B0 only in precipitation, which is taken from ERA-40 reanalysis, while M2 forces the LSS with the entire meteorological ERA-40 dataset. P4 and M1 diverge from B0 for precipitation and the entirety of meteorological fields, respectively, which are from the NCEP–DOE reanalysis product only.

1) P AND M SERIES

Many drainage basins have been submitted to a set of experiments driven by SSiB forced by different precipitation and the entire meteorological conditions. The two series were collected together, since most discharge variation is clearly due to precipitation change. Figure 6 points out this feature: although the amplitudes are different, P1 and M2 show an almost identical phase, and the same can be said of P4 and M1.

It is also evident that the NCEP–DOE reanalysis product, when no relaxation to observations and satellite-based data is applied, leads to a river discharge that is often worse in phase and water volumes than the one driven by ERA-40 alone. The Russian rivers show this behavior (here only Lena discharge is shown; Fig. 6c), but the Amazon (Fig. 6a) also peaks two months before observation in the P4 and M1 cases, whereas P1 and M2 have their maximum only one month early.

The Mississippi (Fig. 6b) shows a poorly represented annual cycle, where the phase is inverted compared to reality both in the baseline experiment and in the sensitivity tests. As GSWP-2-driven discharge does not show such a large discrepancy with observation, there must be a deficiency of SSiB in that area. This is confirmed by the fact that an improved snow and soil parameterization in an improved version of SSiB drives a discharge that is much closer to observation (Z. Guo 2008, personal communication).

Another interesting hint is given by the P2 and P3 experiments, which are forced by hybridized precipitation, without relaxation to remote sensing data. As no correction

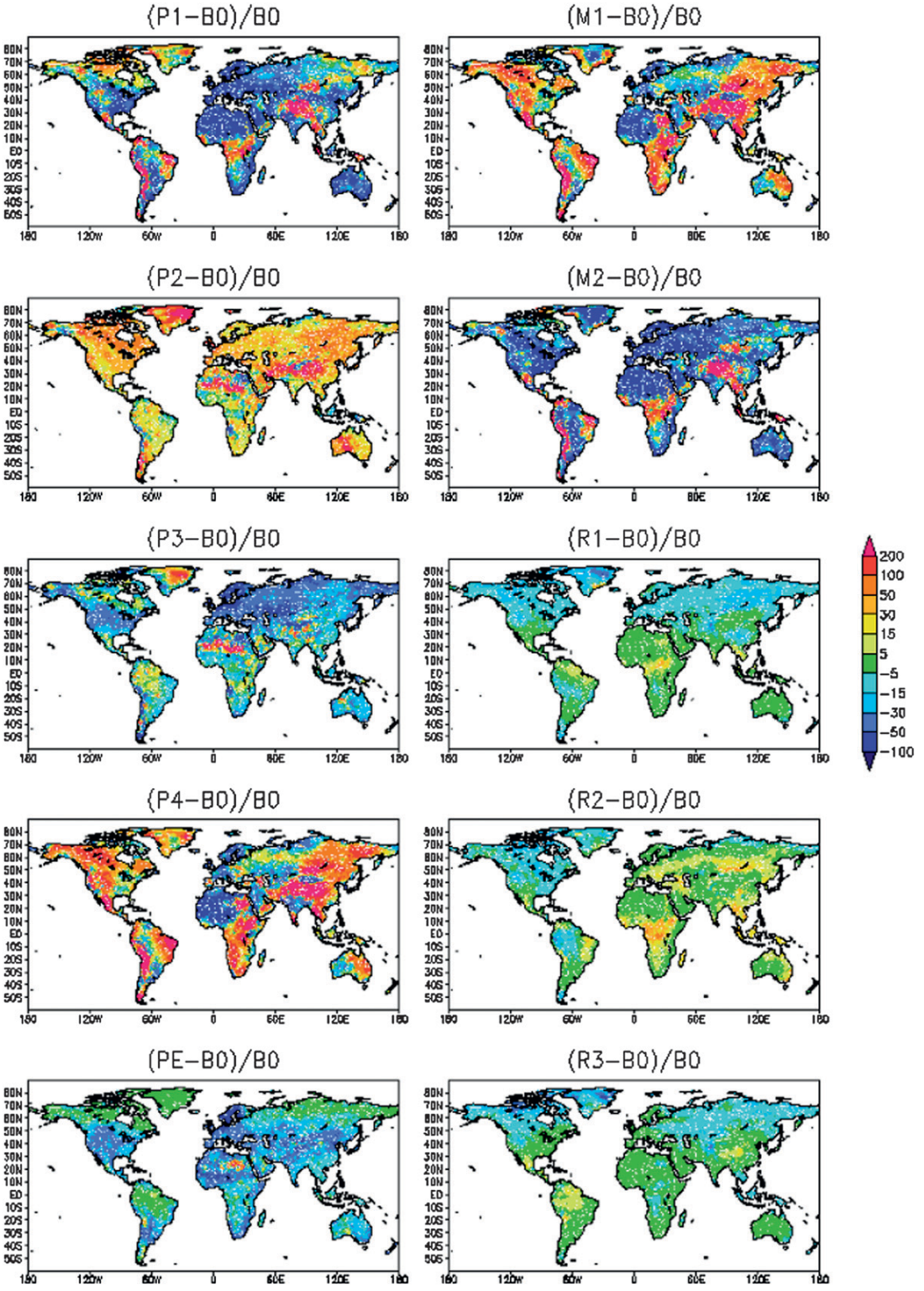

FIG. 5. Differences in gridpoint discharges provided by HD driven by the sensitivity experiments applied to SSiB (see Table 3). Variations are normalized on the baseline test B0 and expressed in percentage.

TABLE 5. Percentage RMS deviation between river discharges forced by P experiments and the baseline test B0, and between R experiments and B0.

	Discharge RMSD P series–baseline	Discharge RMSD R series–baseline
Amazon	0.138	0.085
Mississippi	0.385	0.055
Lena	0.434	0.121
Mackenzie	0.610	0.156
Ganges	0.266	0.036
Chang Jiang	0.724	0.083
Global	0.633	0.065

for wind-caused gauge undercatch is applied to P3, the comparison between the two tests shows the hydrologic impact of neglecting the effect of wind on station data accuracy. It should be noted that correction takes place preferentially at high latitudes and in midlatitude basins characterized by mountainous territory, as the undercatch is predominant for snowfall (Liston and Sturm 2004; Hanson et al. 2004). Moreover, assuming that B0 is the best forcing dataset, the improvement due to undercatch correction is depicted by Fig. 5, which shows less difference between P2 and B0 than between P3 and B0.

To understand the impact of enhanced or decreased precipitation on river discharge, we used a simple sensitivity parameter, which relates the variation of the latter to a change in the former. In this way, we try to understand the response of river discharge to precipitation variability. We define

$$R_X = \frac{(X_{\text{test}} - X_{\text{B0}})}{X_{\text{B0}}}, \tag{8}$$

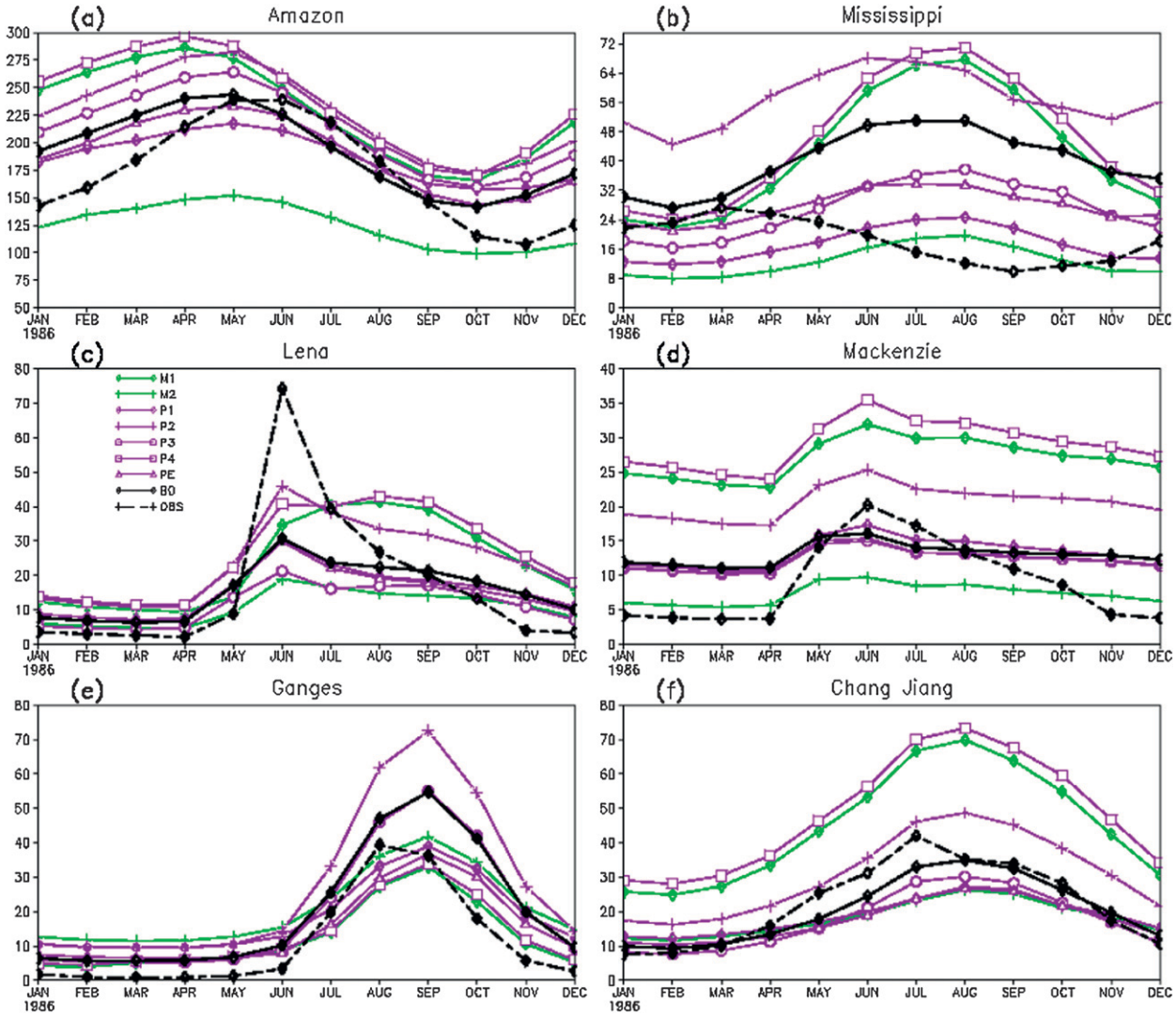

FIG. 6. Discharges for six of the analyzed rivers, simulated with HD forced by SSiB driven by different meteorological and precipitation forcings. All values are expressed in thousands of cubic meters per second.

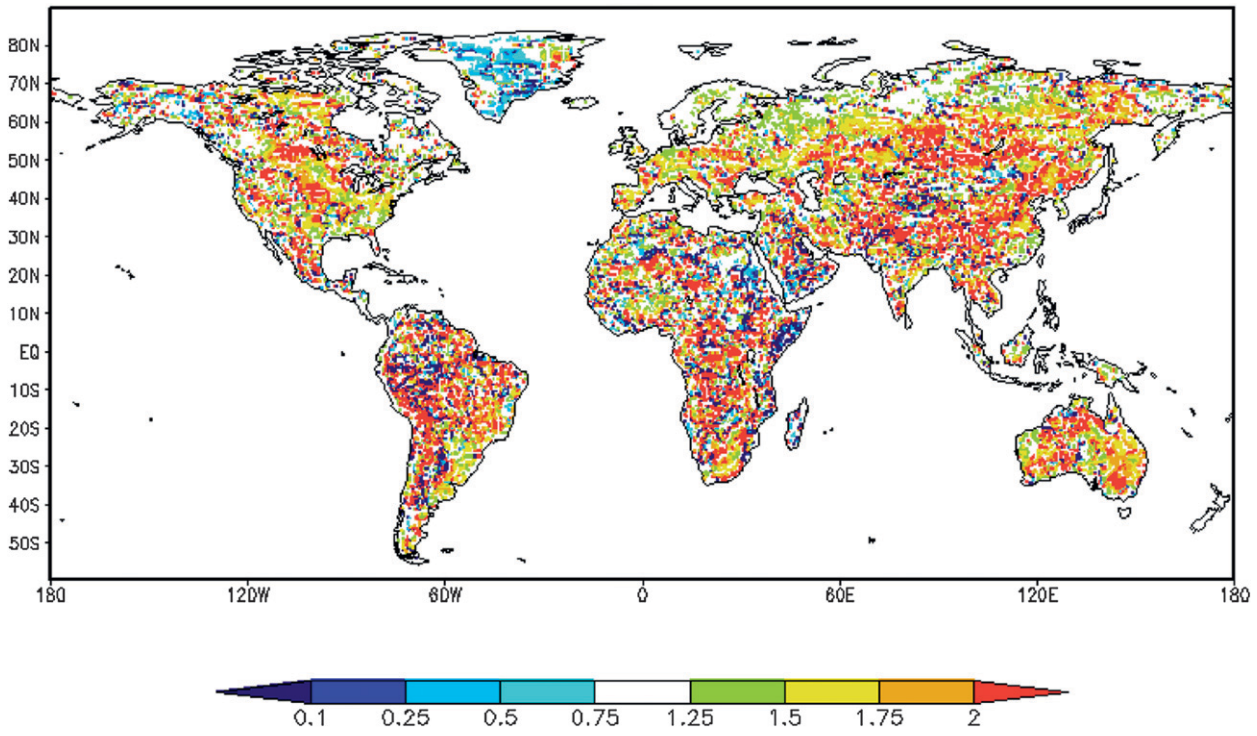

FIG. 7. Ratio S of the variation of discharge d to variation of precipitation p.

where R is the relation parameter between X_{test}, the variable we take into consideration forced by the sensitivity test, and X_{B0}, the same variable driven by the baseline experiment B0. All five normalized differences for discharge and precipitation ($R_{\text{discharge}}$ and R_{precip}) derived for the different precipitation sensitivity tests have been averaged, obtaining two ensemble means $R_{\text{ens discharge}}$ and $R_{\text{ens precip}}$.

The sensitivity of total discharge to precipitation variability would be

$$S_{d,p} = \frac{R_{\text{ens discharge}}}{R_{\text{ens precip}}}, \tag{9}$$

which is displayed in Fig. 7.

Globally, river discharge changes proportionally to a variation of precipitation by an average factor of 2.3, and many areas have runoff extremely sensitive to precipitation ($S_{d,p} \gg 1$). In these locations, a variation of precipitation would lead to a magnified change in runoff, resulting in an amplified response of river discharge. Nearly all the United States looks to be sensitive, and an increase or a reduction of precipitation may considerably impact discharge. All the simulations produce more than 25% increase (decrease) of river flow in response to enhanced (diminished) precipitation, with peaks of 100% in the central United States and the Midwest. Central eastern Asia, except for the Gobi area, appears susceptible, as well as southern Europe and the majority of tropical regions. At high latitudes it is noticeable that a near 1:1 response is predominant; this feature characterizes Scandinavia, northern Canada and Alaska, and most of Siberia. Consequently, boreal region discharge shows the least sensitivity to rainfall variations. This behavior is expected in water-conservative regions that are flat and whose river discharge is mostly driven by spring snow melting.

Desert regions show a less evident signal. Discharge variations directly follow precipitation anomalies in large portions of the Sahara and the Arabian Peninsula. Some of the same regions, instead, show a very small influence of rainfall on discharge (e.g., the Nile drainage basin, where variations between 10% and 75% of the precipitation anomaly are highlighted). Meanwhile, other areas look very susceptible. The Gobi desert is a near 1:1-response region, while central Australia shows strong sensitivity. We assume that such a behavior depends on the very small amount of discharge flowing in those regions, where perturbations in precipitation fields may not be large enough to impact runoff but solely impact evaporation instead.

2) R SERIES

The amplitude of variation in river discharge forced by LSSs driven by different radiation datasets cannot be

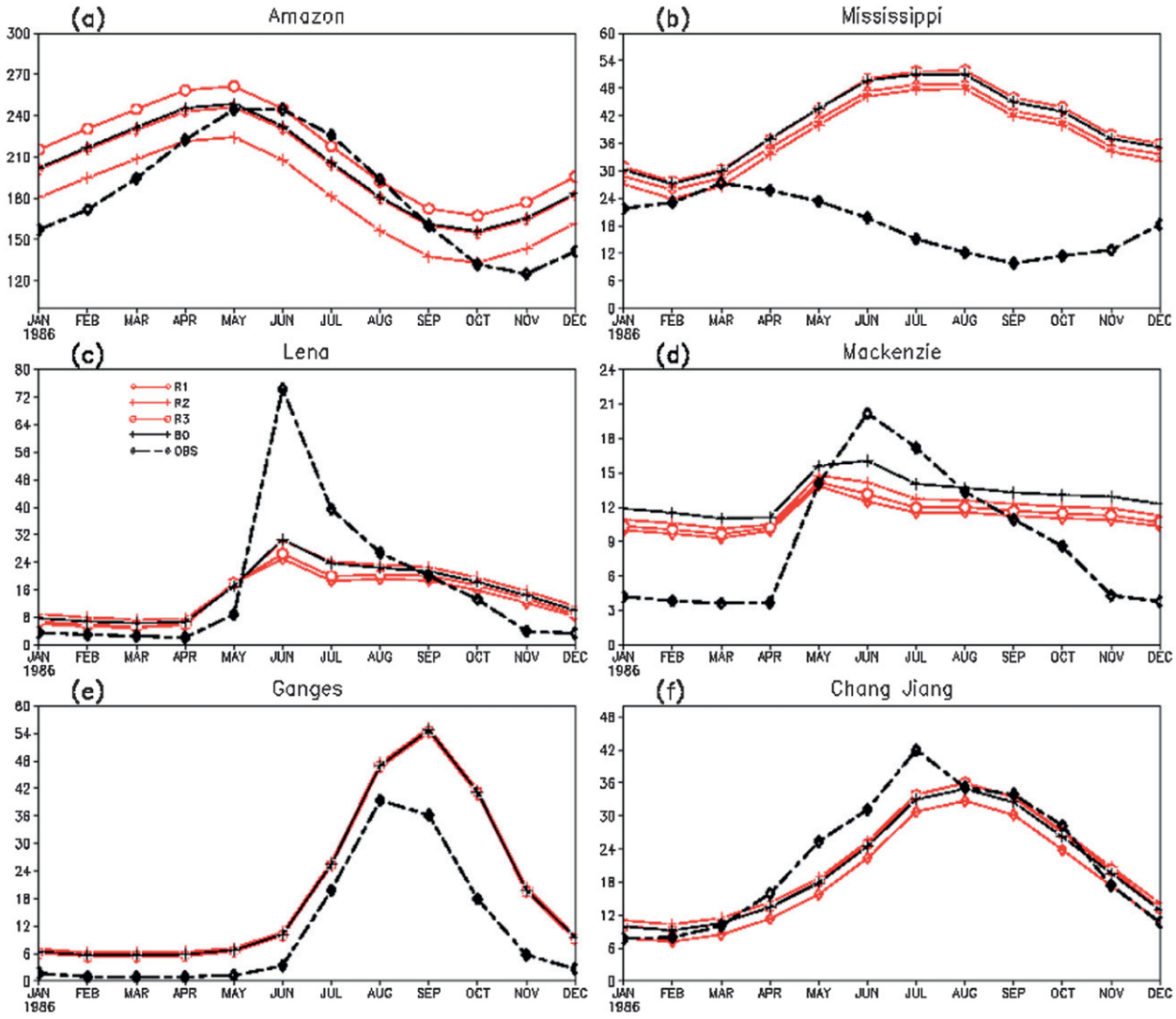

FIG. 8. As in Fig. 6, but driven by different radiation forcings.

neglected. In some cases R tests differ from the baseline experiment by as much as 15%; this occurs in the tropics as well as at high latitudes. Figure 8 depicts the comparison between B0 and R series-driven discharge for the same six rivers represented in Fig. 6. The Lena (Fig. 8c), Congo (not shown), and Mackenzie (Fig. 8d) have the maximum discrepancy from the baseline; whereas the Ganges basin (Fig. 8e) shows no noticeable differences (see also Table 5). Figure 9a explains these patterns by depicting differences between the three radiation tests and the baseline. For instance, Amazon discharge driven by the R1 experiment does not differ much from the one forced by B0 (Fig. 8a) because subbasins where R1 runoff is larger than B0 runoff are counterbalanced by areas where the opposite pattern is verified. On the contrary, in the R2 experiment most of the Amazon watershed's areas generate less runoff than the baseline, and in fact river discharge appears lower than in B0. The opposite pattern can be noticed in the R3-B0 test, resulting in a greater river discharge. Again, the whole set of experiments shows a weaker runoff compared to the baseline in Mackenzie watershed, turning out a lower discharge.

The relationship between runoff and change in surface radiation is further clarified by Fig. 9. First, it should be noted that the main driver is shortwave radiation, while no correlation has been found with longwave. This is reasonable since infrared radiation acts on thermal fluxes whereas shortwave radiation has a direct effect on evaporation (Marshall et al. 2008). Naturally, rainfall that evaporates is deducted from the total runoff balance, and thus a negative correlation is expected between shortwave radiation and runoff.

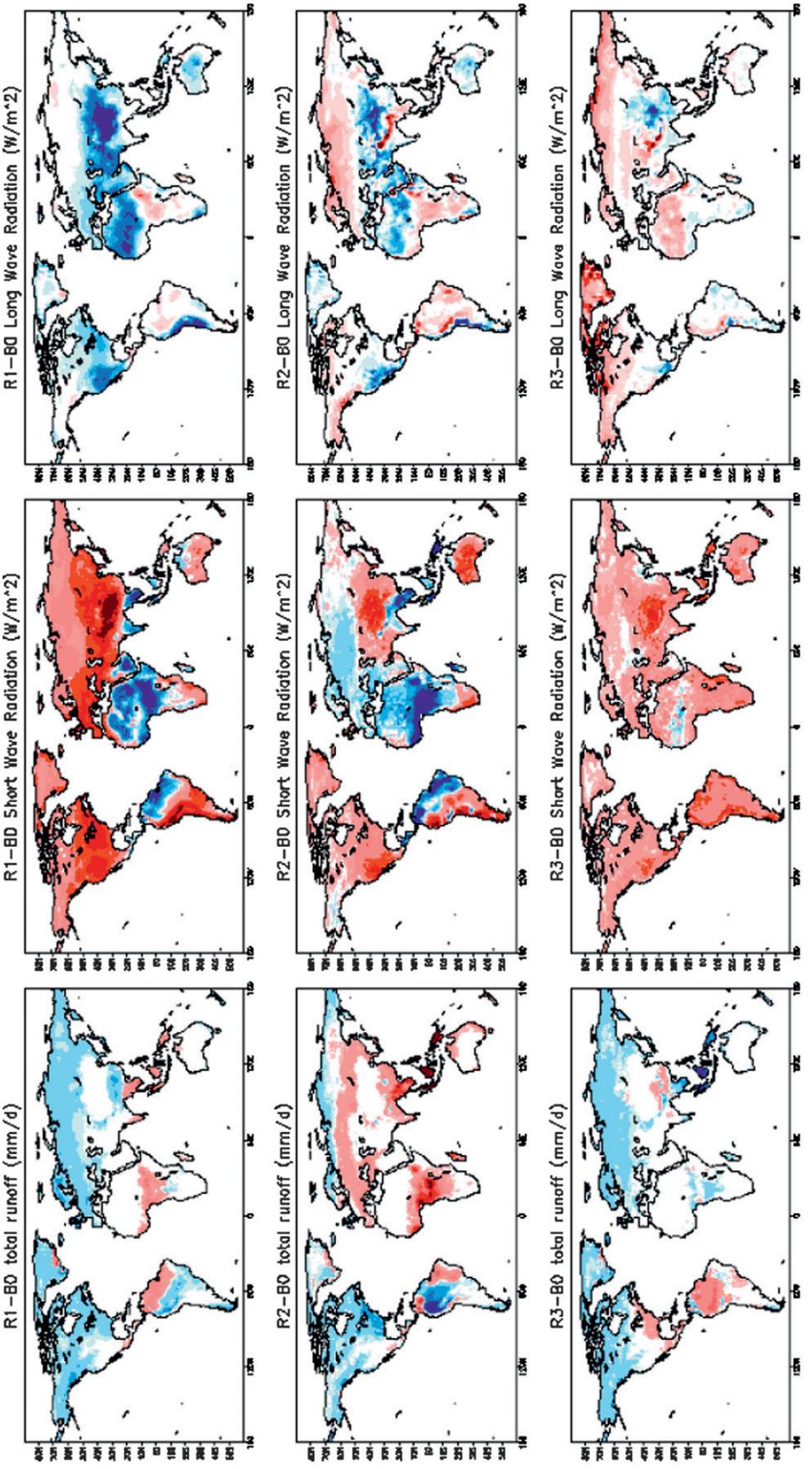

FIG. 9. Annual mean differences between R experiments and baseline (see Table 3) for total runoff, shortwave radiation, and longwave radiation.

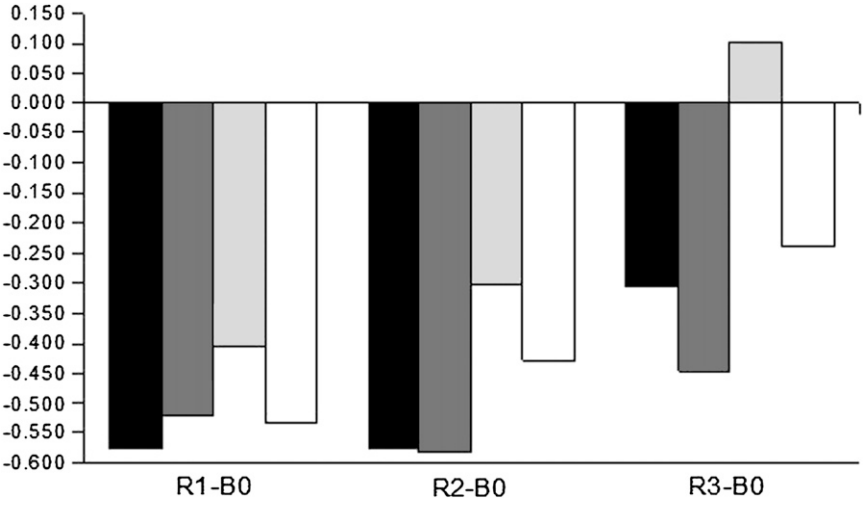

FIG. 10. Correlation coefficients between total runoff and shortwave radiation simulated by SSIB. Each block of bars depicts the difference between the R1, R2, and R3 experiments (see Table 3) and the baseline B0. Black bars represent global correlation, dark gray bars the correlation in the tropics (20°S–20°N), pale gray bars correlation at boreal midlatitudes (20°–55°N), and white bars correlation at high latitudes (55°–85°N). All correlations shown have passed a significance parametric test at 5% level.

The forcing of shortwave radiation does not have the same impact everywhere in the world: for instance, increased radiation in regions where precipitation is very low has little effect on the amount of runoff produced (Fig. 10). For this reason, the midlatitudes show the least negative correlation of discharge with radiation: dry regions like the southwestern United States, the Sahara, and the Gobi have few related patterns. The tropics instead have the highest negative correlation coefficient, and high latitudes show good negative correlations as well. In the R1 and R2 experiments these features are very well represented; in R3 the impact of shortwave radiation is less evident but still globally significant at the 5% level.

6. Summary and conclusions

This study was designed to investigate the response of the HD river routing scheme to different land surface forcing data. First, HD was forced by total runoff from the 13 LSSs taking part in GSWP-2. Afterwards, one of the models (SSiB) was driven by a range of different meteorological inputs and again used to force HD. Both the LSSs and the multimodel analysis provide output fields at 1° resolution, so that a bilinear interpolation is necessary to allow the runoff to fit the 0.5° resolution of the hydrologic model. This operation may represent a limitation of the study because the interpolation does not take into consideration the small-scale spatial variability of runoff. Besides, runoff generated in a catchment at 1° resolution could end up in another drainage basin defined at the HD grid, introducing further error into the estimation of river discharge.

The first part of this study shows that the GSWP-2 MMA generally produces the best phasing of mean annual discharge. However, the contribution of a wide spectrum of LSSs results in a less pronounced seasonal signal of runoff, and curves of annual discharge are flattened. The increasing complexity of the LSS does not always grant for an improved performance of the routing scheme. Sophisticated third-generation land models can have high RMSE, and very simple surface schemes do not drive realistic river flows either. The best capability to drive river routing belongs to second-generation schemes such as Noah and NSIPP, which drive better discharge simulation than the MMA in terms of RMSE.

Some basin discharge estimates are consistently too large because the precipitation forcing to GSWP-2 is overestimated. Furthermore, the HD model does not take into account the impact of human management on water resources; rather, it considers all rivers as natural courses. This might be a limitation in future applications of the river routing scheme with a coupled model.

The second part of this paper examined the response of river discharge to different meteorological forcing data when applied to a single land surface model. Although all the meteorological fields have an effect on river discharge, the role of precipitation is predominant.

Many regions exhibit an enhanced response of discharge to precipitation variance. Our results indicate that

the globally averaged variation of discharge is 2.3 times as large as the change of precipitation. The majority of the United States and central eastern Asia responds more than doubly to a variation of rainfall, and this should be taken into consideration because they are intensely cultivated and inhabited places. For the same reason, the implications of a magnified response to precipitation must be carefully monitored in places like southern Europe ($S_{d,p} > 1.5$). The regional climate projections of the Fourth Assessment Report of the Intergovernmental Panel on Climate Change (IPCC; Solomon et al. 2007) indicate an average 20% reduction of rainfall rates in the Mediterranean region; if this decrease resulted in a magnified response of river flow as shown by our simulation, many millions of people might experience much more severe problems with droughts than foreseen so far. Also, the increase of summer precipitation predicted by the IPCC would have unexpected implications in northern India, Bangladesh, and eastern Asia, some of the most populated and impoverished areas of the entire globe. These results should motivate further assessments of land use and water management adaptation strategies.

Radiation variations also affect river discharge, mainly through the impact of shortwave radiation on evaporation. We found significant negative correlations between solar radiation and total runoff in the tropics and above the 55th parallel, while at midlatitudes the relation is weaker. For our purpose, this correlation can be defined as large, given that only the very direct effect on runoff has been here analyzed. In fact, the implications that radiation variability could have for the whole meteorological system (i.e., its effect on boundary layer growth, convection, etc.) are not considered in this study.

It should also be noted that this part of the study is based on the response of HD to the forcing generated by a single land model. Sensitivity to external meteorological input data may be different for different surface schemes.

Finally, this study exposes some limitations and deficiencies of the HD routing scheme. The static retention time of HD induces errors in discharge simulation for some areas because time-independent velocity does not provide the correct volumes flowing in a drainage area. This occurs especially where large amounts of runoff accumulate in a short time, such as over monsoon regions. The Ganges and Mekong simulated discharges show a peak lag comparable to observations. Mountainous and snowy catchments, where snow melting and steep slopes provoke fast flow velocities, may be affected by the same error, and most simulations display delayed Mississippi discharge both in the minimum and the maximum. The introduction of a dynamic delay time should improve the phase of the simulated discharge.

Acknowledgments. Stefano Materia would like to thank the whole Center for Ocean–Land–Atmosphere Studies for inviting him to spend six months as a visiting student. He is particularly grateful to the COLA land surface group, whose contributions were fundamental to the earlier stages of the study.

REFERENCES

Alessandri, A., and A. Navarra, 2008: On the coupling between vegetation and rainfall inter-annual anomalies: Possible contributions to seasonal rainfall predictability over land areas. *Geophys. Res. Lett.,* **35,** L02718, doi:10.1029/2007GL032415.

——, S. Gualdi, J. Polcher, and A. Navarra, 2007: Effects of land surface–vegetation on the boreal summer surface climate of a GCM. *J. Climate,* **20,** 255–278.

AMS Council, 2001: Statement on seasonal to interannual climate prediction. *Bull. Amer. Meteor. Soc.,* **82,** 701–703.

Barros, V., L. Chamorro, G. Coronel, and J. Baez, 2004: The major discharge events in the Paraguay River: Magnitudes, source regions, and climate forcings. *J. Hydrometeor.,* **5,** 1161–1170.

Bonan, G. B., K. W. Oleson, M. Vertenstein, S. Levis, X. Zeng, Y. Dai, R. E. Dickinson, and Z.-L. Yang, 2002: The land surface climatology of the Community Land Model coupled to the NCAR Community Climate Model. *J. Climate,* **15,** 3123–3149.

Branstetter, M. L., and D. J. Erickson, 2003: Continental runoff dynamics in the Community Climate System Model 2 (CCSM2) control simulation. *J. Geophys. Res.,* **108,** 4550, doi:10.1029/2002JD003212.

Decharme, B., and H. Douville, 2007: Global validation of the ISBA sub-grid hydrology. *Climate Dyn.,* **29,** 21–37.

Dirmeyer, P. A., and F. J. Zeng, 1999: An update to the distribution and treatment of vegetation and soil properties in SSiB. Centre for Land–Ocean–Atmosphere Studies Tech. Rep. 78, 25 pp.

——, and L. Tan, 2001: A multi-decadal global land-surface data set of state variable and fluxes. Centre for Land–Ocean–Atmosphere Studies Tech. Rep. 102, 43 pp. [Available online at http://grads.iges.org/pubs/ctr_102.pdf.]

——, X. Gao, M. Zhao, Z. Guo, T. Oki, and N. Hanasaki, 2006: GSWP-2: Multimodel analysis and implication for our perception of the land surface. *Bull. Amer. Meteor. Soc.,* **87,** 1381–1397.

Ducharne, A., R. D. Koster, M. J. Suarez, M. Stieglitz, and P. Kumar, 2000: A catchment-based approach to modeling land surface processes in a general circulation model. Part 2: Parameter estimation and model demonstration. *J. Geophys. Res.,* **105** (D20), 24 823–24 838.

Edwards, M. O., 1989: Global gridded elevation and bathymetry on 5-minute geographic grid (ETOPO5): Digital raster data on a 5-minute geographic (lat/long) 2160x4320 (centroid-registered) grid. NOAA, National Geophysical Data Center.

Ek, M. B., K. E. Mitchell, Y. Lin, P. Grunmann, E. Rogers, G. Gayno, V. Koren, and J. D. Tarpley, 2003: Implementation of Noah land surface model advances in the National Centers for Environmental Prediction operational mesoscale Eta model. *J. Geophys. Res.,* **108,** 8851, doi:10.1029/2002JD003296.

Essery, R. L. H., M. J. Best, R. A. Betts, P. M. Cox, and C. M. Taylor, 2003: Explicit representation of subgrid heterogeneity in a GCM land surface scheme. *J. Hydrometeor.,* **4,** 530–543.

Etchevers, P., C. Colaz, and F. Habets, 2001: Simulation of the water budget and the rivers flows of the Rhone basin from 1981 to 1994. *J. Hydrol.,* **244,** 60–85.

Ferranti, L., and P. Viterbo, 2006: The European summer of 2003: Sensitivity to soil water initial conditions. *J. Climate,* **19,** 3659–3680.

Fischer, E. M., S. Seneviratne, D. Lüthi, and C. Schär, 2007: Contribution of land–atmosphere coupling to recent European summer heat waves. *Geophys. Res. Lett.,* **34,** L06707, doi:10.1029/2006GL029068.

Guo, Z., and P. A. Dirmeyer, 2006: Evaluation of the Second Global Soil Wetness Project soil moisture simulations: 1. Intermodel comparison. *J. Geophys. Res.,* **111,** D22S02, doi:10.1029/2006JD007233.

——, ——, Z.-Z. Hu, X. Gao, and M. Zhao, 2006: Evaluation of the Second Global Soil Wetness Project soil moisture simulations: 2. Sensitivity to external meteorological forcing. *J. Geophys. Res.,* **111,** D22S03, doi:10.1029/2006JD007845.

Gusev, Y. M., and O. N. Nasonova, 2003: The simulation of heat and water exchange in the boreal spruce forest by the land-surface model SWAP. *J. Hydrol.,* **280,** 162–191.

Hagemann, S., and L. Dümenil, 1998a: A parametrization of lateral waterflow for the global scale. *Climate Dyn.,* **14,** 17–41.

——, and ——, 1998b: Documentation for the Hydrological Discharge Model. Max Planck Institute for Meteorology Tech. Rep. 17, 42 pp.

Hall, F. G., and Coauthors, 2006: The ISLSCP Initiative II global data sets: Surface boundary conditions and atmospheric forcings for land-atmosphere studies. *J. Geophys. Res.,* **111,** D22S01, doi:10.1029/2006JD007366.

Hanasaki, N., S. Kanae, and T. Oki, 2006: A reservoir operation scheme for global river routing models. *J. Hydrol.,* **327,** 22–41.

——, ——, ——, K. Masuda, K. Motoya, N. Shirakawa, Y. Shen, and K. Tanaka, 2008: An integrated model for the assessment of global water resources—Part 1: Model description and input meteorological forcing. *Hydrol. Earth Syst. Sci.,* **12,** 1007–1025.

Hanson, C. L., F. B. Pierson, and G. L. Johnson, 2004: Dual-gauge system for measuring precipitation: Historical development and use. *J. Hydrol. Eng.,* **9,** 350–359.

Huffman, G. J., and Coauthors, 1997: The Global Precipitation Climatology Project (GPCP) combined precipitation dataset. *Bull. Amer. Meteor. Soc.,* **78,** 5–20.

Kanamitsu, M., W. Ebisuzaki, J. Woollen, S. K. Yang, J. J. Hnilo, M. Fiorino, and G. L. Potter, 2002: NCEP–DOE AMIP-II reanalysis (R-2). *Bull. Amer. Meteor. Soc.,* **83,** 1631–1648.

Koster, R. D., and M. J. Suarez, 1992: Modeling the land surface boundary in climate models as a composite of independent vegetation stands. *J. Geophys. Res.,* **97** (D3), 2697–2715.

——, ——, A. Ducharne, M. Stieglitz, and P. Kumar, 2000: A catchment-based approach to modeling land surface processes in a general circulation model. 1. Model structure. *J. Geophys. Res.,* **105** (D20), 24 809–24 822.

——, and Coauthors, 2006: GLACE: The Global Land–Atmosphere Coupling Experiment. Part I: Overview. *J. Hydrometeor.,* **7,** 590–610.

Krinner, G., and Coauthors, 2005: A dynamic global vegetation model for studies of the coupled atmosphere–biosphere system. *Global Biogeochem. Cycles,* **19,** GB1015, doi:10.1029/2003GB002199.

Liston, G. E., and M. Sturm, 2004: The role of winter sublimation in the Arctic moisture budget. *Nord. Hydrol.,* **35,** 325–334.

Manabe, S., 1969: Climate and the ocean circulation. I. The atmospheric circulation and the hydrology of the earth's surface. *Mon. Wea. Rev.,* **97,** 739–774.

Marshall, A. G., O. Alves, and H. H. Hendon, 2008: An enhanced moisture convergence–evaporation feedback mechanism for MJO air–sea interaction. *J. Atmos. Sci.,* **65,** 970–986.

Milly, P. C. D., and A. B. Shmakin, 2002a: Global modeling of land water and energy balances. Part I: The Land Dynamics (LaD) model. *J. Hydrometeor.,* **3,** 283–299.

——, and ——, 2002b: Global modeling of land water and energy balances. Part II: Land characteristic contributions to spatial variability. *J. Hydrometeor.,* **3,** 301–310.

Mocko, D. M., and Y. C. Sud, 2001: Refinements to SSiB with an emphasis on snow physics: Evaluation and validation using GSWP and Valdai data. *Earth Interactions,* **5.** [Available online at http://EarthInteractions.org.]

Niu, G.-Y., and L. Yang, 2003: The versatile integrator of surface atmospheric processes. Part II: Evaluation of three topography-based runoff schemes. *Global Planet. Change,* **38,** 191–208.

Oki, T., T. Nishimura, and P. A. Dirmeyer, 1999: Assessment of annual runoff from land surface models using Total Runoff Integrating Pathways (TRIP). *J. Meteor. Soc. Japan,* **77,** 235–255.

Robock, A., K. Y. Vinnikov, G. Srinivasan, J. K. Entin, S. E. Hollinger, N. A. Speranskaya, S. Liu, and A. Namkhai, 2000: The global soil moisture data bank. *Bull. Amer. Meteor. Soc.,* **81,** 1281–1299.

Roeckner, E., and Coauthors, 2003: The atmospheric general circulation model ECHAM5, part I. Max-Planck-Institut für Meteorologie Rep. 349, 127 pp.

Rossow, W. B., and Y. C. Zhang, 1995: Calculation of surface and top of atmosphere radiative fluxes from physical quantity based on ISCCP data sets: 2. Validation and first results. *J. Geophys. Res.,* **100,** 1167–1197.

Rudolf, B., H. Hauschild, W. Reuth, and U. Schneider, 1994: Terrestrial precipitation analysis: Operational method and required density of point measurement. *Global Precipitation and Climate Change,* M. Desbois and F. Desalmand, Eds., Springer, 173–186.

Simmons, A. J., and J. K. Gibson, 2000: The ERA-40 project plan. ECMWF, ERA-40 Proj. Rep., Ser. 1, 63 pp. [Available online at http://www.ecmwf.int/publications/library/ecpublications/_pdf/ERA40_PRS_1.pdf.]

Singh, V. P., 1988: *Rainfall-Runoff Modelling*. Vol. 1, *Hydrologic Systems.* Prentice Hall, 480 pp.

Solomon, S., D. Qin, M. Manning, M. Marquis, K. Averyt, M. M. B. Tignor, H. L. Miller Jr., and Z. Chen, Eds., 2007: *Climate Change 2007: The Physical Sciences Basis*. Cambridge University Press, 996 pp.

Stackhouse, P. W., Jr., S. K. Gupta, S. J. Cox, M. Chiacchio, and J. C. Mikovitz, 2000: The SRB project release 2 data set: An update. *GEWEX News,* No. 10, International GEWEX Project Office, Silver Spring, MD, 4.

Takeuchi, K., 2001: Increasing vulnerability to extreme floods and societal needs of hydrological forecasting. *Hydrol. Sci. J.,* **46,** 869–881.

Vörösmarty, C. J., and D. Sahagian, 2000: Anthropogenic disturbance of the terrestrial water cycle. *Bioscience,* **50,** 753–765.

Xue, Y., P. J. Sellers, J. L. Kinter, and J. Shukla, 1991: A simplified biosphere model for global climate studies. *J. Climate,* **4,** 345–364.

Yang, Z.-L., and G.-Y. Niu, 2003: The versatile integrator of surface and atmosphere processes. Part I: Model description. *Global Planet. Change,* **38,** 175–189.

Zeng, N., A. Mariotti, and P. Wetzel, 2005: Terrestrial mechanisms of interannual CO_2 variability. *Global Biogeochem. Cycles,* **19,** GB1016, doi:10.1029/2004GB002273.

Zhao, M., and P. Dirmeyer, 2003: Production and analysis of GSWP-2 near-surface meteorology data sets. COLA Technical Report 159, 22 pp. [Available online at ftp://grads.iges.org/pub/ctr/ctr_159.pdf.]